Acta Biomaterialia xxx (xxxx) xxx

Contents lists available at ScienceDirect

Acta Biomaterialia

journal homepage: www.elsevier.com/locate/actabiomat

Full length article

A bioink blend for rotary 3D bioprinting tissue engineered small-diameter vascular constructs ☆

Sebastian Freeman [a,b], Rafael Ramos [c], Paul Alexis Chando [c], Luxi Zhou [a,b], Kyle Reeser [a,b], Sha Jin [a,b], Pranav Soman [c], Kaiming Ye [a,b,*,1]

[a] Department of Biomedical Engineering, Watson School of Engineering and Applied Science, State University of New York (SUNY), Binghamton, NY 13902, United States
[b] Center of Biomanufacturing for Regenerative Medicine, Binghamton University, State University of New York (SUNY), Binghamton, NY 13902, United States
[c] Department of Biomedical and Chemical Engineering, Syracuse Biomaterials Institute, Syracuse University, Syracuse, NY 13210, United States

ARTICLE INFO

Article history:
Received 20 January 2019
Received in revised form 19 June 2019
Accepted 26 June 2019
Available online xxxx

Keywords:
3D bioprinting
Additive biomanufacturing
Vessel substitutes
Vascular engineering
Vessel bioprinting

ABSTRACT

3D bioprinted vascular constructs have gained increased interest due to their significant potential for creating customizable alternatives to autologous vessel grafts. In this study, we developed a new approach for biofabricating fibrin-based vascular constructs using a novel rotary 3D bioprinter developed in our lab. We formulated a new bioink by incorporating fibrinogen with gelatin to achieve a desired shear-thinning property for rotary bioprinting. The blending of heat-treated gelatin with fibrinogen turned unprintable fibrinogen into a printable biomaterial for vessel bioprinting by leveraging the favorable rheological properties of gelatin. We discovered that the heat-treatment of gelatin remarkably affects the rheological properties of a gelatin-fibrinogen blended bioink, which in turn influences the printability of the ink. Further characterizations revealed that not only concentration of the gelatin but the heat treatment also affects cell viability during printing. Notably, the density of cells included in the bioinks also influenced printability and tissue volumetric changes of the printed vessel constructs during cultures. We observed increased collagen deposition and construct mechanical strength during two months of the cultures. The burst pressure of the vessel constructs reached 1110 mmHg, which is about 52% of the value of the human saphenous vein. An analysis of the tensile mechanical properties of the printed vessel constructs unveiled an increase in both the circumferential and axial elastic moduli during cultures. This study highlights important considerations for bioink formulation when bioprinting vessel constructs.

Statement of Significance

There has been an increased demand for small-diameter tissue-engineered vascular grafts. Vascular 3D bioprinting holds the potential to create equivalent vascular grafts but with the ability to tailor them to meet patient's needs. Here, we presented a new and innovative 3D rotary bioprinter and a new bioink formulation for printing vascular constructs using fibrinogen, a favorable biomaterial for vascular tissue engineering. The bioink was formulated by blending fibrinogen with a more printable biomaterial, gelatin. The systematic characterization of the effects of heat treatment and gelatin concentration as well as bioink cell concentration on the printability of the bioink offers new insight into the development of printable biomaterials for tissue biofabrication.

1. Introduction

Cardiovascular diseases (CVDs), such as coronary artery disease (CAD) and peripheral artery disease (PAD) are considered as the number one cause of death globally [1]. CAD treatment includes medical therapy and endovascular interventions. Endovascular therapies offer a lower risk option over open surgery grafting. Studies indicate that multiple coronary bypass graft implantation

☆ Part of the Cell and Tissue Biofabrication Special Issue, edited by Professors Guohao Dai and Kaiming Ye.

* Corresponding author at: Department of Biomedical Engineering, Watson School of Engineering and Applied Sciences, Binghamton University, State University of New York (SUNY), PO Box 6000, Binghamton, NY 13902, United States.
E-mail address: kye@binghamton.edu (K. Ye).

[1] Guest editors did not participate in, or have access to, the peer-review process for manuscripts on which they were an author.

https://doi.org/10.1016/j.actbio.2019.06.052
1742-7061/

could reroute the blood around the clogged artery to supply blood to the heart [2–5], highlighting the need for improved graft options. Synthetic grafts made from Dacron and ePTFE have been used since the 1970s. These biomaterials are more promising for fabricating large (>8 mm) or medium diameter (6–8 mm) grafts [6]. Recent advance in vascular tissue engineering has produced novel synthetic grafts for small (<6 mm) diameter applications [7–10]. Autologous arteries or veins are, however, still the favored conduits for revascularization through grafting. The internal thoracic artery, radial artery, and saphenous vein (SV) are the most commonly used autologous grafts [6,11,12]. Despite representing the gold standard, SV patency rates remain low, showing a failure rate around 50% at 10 years [13]. Grafts taken from other parts of the body are rarely optimal in dimensions or their mechanical properties resulting in compliance mismatch at the graft site, one of the leading causes of intimal hyperplasia and graft failure [14,15].

Tissue-engineered vascular grafts (TEVGs) have been increasingly explored as alternatives due to their potential to replace the autologous grafts. TEVGs remodeled by cells *in vitro* can be engineered to achieve an *in vivo* burst pressure and extracellular matrix (ECM) composition similar to autologous grafts [16–19]. Small diameter grafts are more susceptible to the loss of patency caused by thrombosis [20], which can be overcome through endothelialization or surface modification of the luminal surface to bestow anti-thrombotic properties on to the grafts [21]. Several approaches have been developed to create TEVGs in the last two decades. This includes the use of collagen [22–28] and fibrinogen [18,29–37] to cast TEVGs using molds. Scaffold-free approaches have also been attempted [38–40]. Cell sheet fabrication is another technology that has been developed lately for fabricating TEVGs, where cells such as fibroblasts or smooth muscle cells can be grown to confluence and then lifted off as a sheet to be rolled into TEVGs [16,17,41,42]. However, these methods have limitations for creating on-demand tissue constructs and recapitulating complexed tissue structures of a vessel. Casting approaches require different molds when different dimensions are desired and are unable to recreate the distinct regions of the tunica externa, media, and intima of arteries. Cell sheet technology requires culturing many cell sheets to accumulate sufficient numbers in order to create a single TEVG.

3D bioprinting is a novel technology that has attracted attentions due to its potential to create on-demand tissue-engineered products. Over the last several years, many groups have reported functional tissues and organs manufactured by 3D bioprinting such as skin [43–47], liver [48,49], kidney [50] and proximal tubules [51], and muscles [52–55]. A number of biomaterials including collagen and fibrinogen have been explored for constructing TEVGs. Collagen bioinks have been tested for 3D bioprinting but require the use of very high concentrations in order to retain their shape during printing [56]. Alginate can be a good biomaterial for fabricating TEVGs due to its good printability to create a layer-by-layer organization of blood vessels [57–59]. However, it is inherently bioinert, and requires mixing with other biomaterials or chemical modification to improve cell attachment [60]. Fibrinogen promotes *de novo* collagen synthesis, making it an attractive biomaterial for fabricating TEVGs [30,61]. Its low viscosity makes it unfit for 3D bioprinting. Gelatin, the hydrolyzed derivative of collagen, is another commonly used biomaterial for 3D bioprinting due to its well-established thermoreversible properties. It forms a gel at a low temperature; but it becomes a liquid at 37 °C. Gelatin is primarily composed of subunits of native collagen α-chains. It also contains higher molecule weight fractions with multiple crosslinks (β- and γ-chains). Degradation of these chains begins at temperatures higher than 40 °C at which point lower molecular weight fractions form [62]. The change of the molecular weight affects gelatin's functionality considerably [63–65]. Gelatin has been used in combination with other biomaterials for constituting various bioinks [46,51,52,66–69].

We herein present a new technology for formulating a novel bioink for biofabricating TEVGs using a rotary 3D bioprinter developed in our lab. We blended gelatin with fibrinogen to formulate a bioink with a favorable rheological property and printability for generating vessel constructs whose biomechanical properties improve during cultures. This new bioink overcomes the limitations of incorporating a favorable biomaterial such as fibrinogen that does not have the desired rheological characteristics for extrusion bioprinting.

We hypothesized that the inclusion of the gelatin in a fibrinogen bioink would impart the rheological properties of a gel to the blended bioink. A gelatin gel, unlike viscous liquids, does not deform due to gravity. It encapsulates the soluble fibrinogen and cells during printing and subsequent enzymatic crosslinking of the fibrinogen by thrombin. Furthermore, we hypothesized that the fibrin network maintains its printed construct when gelatin is vacated from the fibrin fiber network. The development of this new bioink enables the use of one of the favorable biomaterials, i.e. fibrinogen for biofabricating TEVGs.

2. Materials and methods

2.1. The configuration of a rotary 3D bioprinter for fabricating TEVGs

We developed a three-axis rotary 3D bioprinter with z-, r-, and θ-axes for fabricating TEVGs, as shown in Fig. 1A. The printer is controlled by an Arduino Mega 2560 microcontroller board loaded with an open-source Marlin firmware. To print a TEVG, a polystyrene rod whose diameter matches the inner diameter of a desired vascular graft is held by a coupler and rotated by a NEMA 17 stepper motor mounted on a movable stage. An extrusion system utilizing a syringe was on a fourth, NEMA 14 stepper motor-controlled axis. Extrusion flow rates ranged from 1 to 7 mL/min out of a 24 G (0.330 mm ID) polypropylene tapered extrusion tip Jensen Global (Santa Barbara, CA). Tips were autoclaved at 121 °C before use.

2.2. The preparation of bioinks and cells for TEVG printing

To prepare a bioink for fabricating TEVGs using a rotary 3D bioprinter, we mixed fibrinogen with gelatin after heat treatment. Gelatin from porcine skin (type-A, 300 bloom, 500–1000 kDa) (Sigma-Aldrich) was dissolved in the Dulbecco's phosphate buffered saline (DPBS) without calcium and magnesium (Corning, NY) to a concentration of 15% (w/v) and heated in a hot water bath at 90 °C. After heat treatment, the warm gelatin was sterile-filtered and stored at 4 °C. A stock solution of 60 mg/mL fibrinogen from bovine plasma (Sigma-Aldrich) (65–85% protein, ≥75% clottable protein) was prepared by layering over warm DPBS and incubating for 12 h at 37 °C. After incubation, the fibrinogen stock was filtered first through a 0.45-μm nylon filter and subsequently through a 0.2-μm regenerated cellulose filter. Fibrinogen stocks were stored at −20 °C until use.

To prepare a cell-laden bioink, we mixed low passage primary neonatal human dermal fibroblasts (HDF-n) (ScienCell Research Laboratories Inc.) into the gelatin-fibrinogen bioink for printing. HDF-n were cultured in a high glucose (4.5 g/L) DMEM supplemented with 4 mM L-glutamine, 1 mM sodium pyruvate, 10% (v/v) fetal bovine serum (FBS) (Sigma-Aldrich), and 1% (v/v) penicillin-streptomycin in 5% CO_2 and 37 °C. The culture medium was exchanged every 2–3 days. The cells were passaged by trypsin-EDTA (Carlsbad, CA) treatment when they reached

Please cite this article as: S. Freeman, R. Ramos, P. Alexis Chando et al., A bioink blend for rotary 3D bioprinting tissue engineered small-diameter vascular constructs, Acta Biomaterialia, https://doi.org/10.1016/j.actbio.2019.06.052

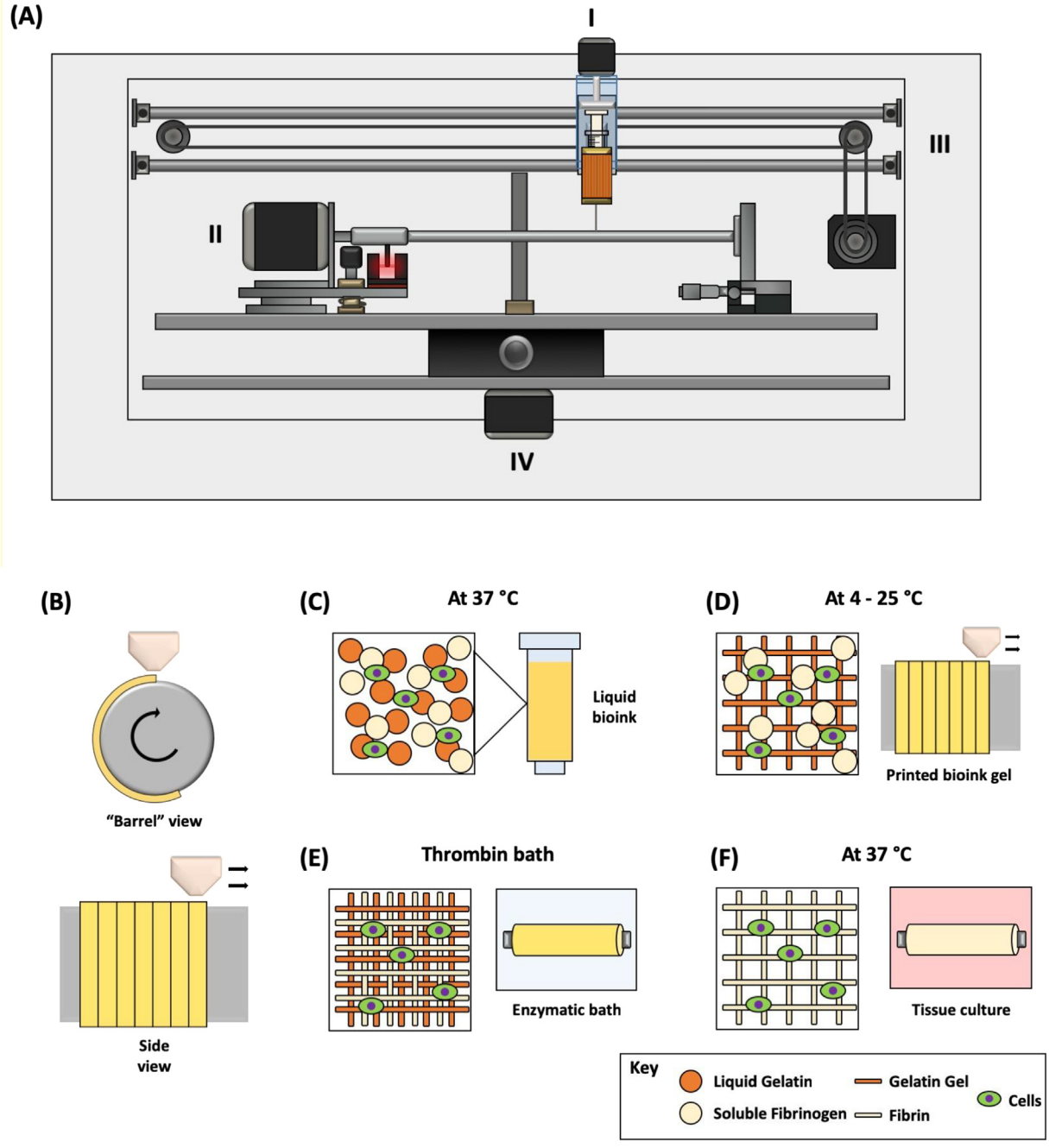

Fig. 1. Biofabrication of tissue engineered vascular constructs using a rotary 3D bioprinter. (A) A diagram of a rotary 3D bioprinter. Symbols: I) Motor-controlled extruder, II) Motor-controlled mandrel, III) Motor-controlled z-axis, and IV) movable stage. (B) 3D bioprinting process on a rotating surface. A cell-laden hydrogel is extruded from a syringe extrusion head onto a rotating rod while the extrusion head proceeds linearly along the axis of the rod. (C) Gelatin, fibrinogen, and cells are mixed together at 37 °C, and loaded into a syringe. (D) Cell-laden bioink is chilled rapidly to gel gelatin and to encapsulate fibrinogen and cells in a well-mixed state. After warming the bioink to 23–25 °C, the gel is printed helically around the rod. (E) The printed vascular construct is submerged in a thrombin bath to crosslink the fibrinogen. (F) The vascular construct is placed in a CO_2 incubator for culture. The gelatin is vacated from the construct during the culture.

80–90% confluence. Passages lower than 10 were used for printing experiments. Before incorporating into the bioink, the HDF-n cell pellets were re-suspended in a DPBS (without calcium or magnesium) supplemented with 20 mM HEPES (2-[4-(2-hydroxyethyl) piperazin-1-yl] ethane sulfonic acid) (Life Technologies, Carlsbad, CA) and 1% (v/v) FBS.

A stock solution of 2000 U/mL thrombin (Alfa Aesar, Haverhill, MA) was prepared for fibrinogen crosslinking. Ethidium homodimer-1 fluorescent dye was employed to determine the cell viability within printed vessel constructs after printing. A portion of 30 μL of a cell-laden bioink was printed in triplicate into the wells of a 96-well plate and subsequently stained with ethidium homodimer-1 and examined using a plate reader at 530 nm and 645 nm to quantify its fluorescence intensity. The entire well was scanned by the plate reader, so the intensity value analyzed for each replicate is the average spatial intensity for the whole well.

TEVGs were printed using cell-laden (containing either 1 or 3×10^6 cells/mL) bioink that was composed of 7.5% (w/v) gelatin and 10 mg/mL fibrinogen. The printed constructs had approximate initial dimensions of 20 mm (L) × 4.9 mm (ID) × 10.9 mm (OD).

Please cite this article as: S. Freeman, R. Ramos, P. Alexis Chando et al., A bioink blend for rotary 3D bioprinting tissue engineered small-diameter vascular constructs, Acta Biomaterialia, https://doi.org/10.1016/j.actbio.2019.06.052

Constructs were printed onto a polystyrene rod that had been pre-treated with 10% (w/v) Pluronic F-127 (Sigma-Aldrich) for 1 h and then air-dried. The constructs were placed in a custom-made PDMS chamber with 8 mL of the cell culture medium supplemented with 50 μg/mL L-ascorbate (Sigma-Aldrich) to enhance the secretion of collagen from derma fibroblasts. To maintain cell-secreted soluble factors, only half the medium was exchanged every two days with 100 μg/mL L-ascorbate.

2.3. Fibrin network formation

For a better understanding of fibrinogen crosslinking, a dye-conjugated fibrinogen was prepared by NHS chemistry. Briefly, 250 mg of bovine fibrinogen was dissolved in 25 mL of 50 mM borate buffer, pH 8.5, to form a 10 mg/mL solution. *N*-hydroxysuccinimide (Thermo Scientific) conjugated with rhodamine (Thermo Scientific) was added at a 10:1 M ratio of dye/fibrinogen. After reacting for 2 h at room temperature, the dye-fibrinogen was dialyzed in a 6–8 kDa membrane filter against a 1 L bath of PBS for 3 days. The PBS in the bath was exchanged twice a day. After dialysis, the labeled fibrinogen was frozen at −80 °C, lyophilized, and stored at −20 °C until use. Stocks of 60 mg/mL rhodamine-fibrinogen were reconstituted in DPBS. Gelatin solutions were mixed with 10 mg/mL rhodamine-fibrinogen chilled to 4 °C, allowed to warm up to room temperature, crosslinked with 1 U/mL thrombin overnight, and then visualized under a Zeiss LSM 880 laser confocal scanning microscope using a 63× oil immersion objective.

2.4. Rheological measurements

The rheological properties of the bioinks were analyzed using a rotational rheometer (ARES G2, TA Instruments). All solutions were well-mixed at 37 °C, chilled to 4 °C to gel, and then allowed to warm up to room temperature for testing. For determining the viscosity profiles, each sample was tested in a shear ramp test running from 0.1 s^{-1} to 100 s^{-1} shear rate. The range of tested shear rates was chosen in order to include potentially relevant shear rates created as the bioink was extruded. Assuming an incompressible Newtonian fluid, for an average flow velocity of 100 mm/min and an extrusion tip diameter of 0.330 mm, shear rate values around 40 s^{-1} would be expected. For determining the storage moduli of the bioink, an oscillation frequency of 0.1 Hz was used. All samples were run in triplicate.

2.5. Scanning electron microscopy (SEM) and cryomicroscopy (cryoSEM)

The effects of heat treatment and gelatin concentration on printability of the bioinks were characterized by either SEM or cryoSEM. Different bioinks as described above were examined after printing. For SEM, a bioink sample was placed in a 7 × 7 × 5 mm plastic mold and flash frozen in liquid nitrogen for 2 min, followed by freeze-drying for 48 h. Dried samples were carbon-coated with a carbon coater (Cressington 208C, Cressington Scientific Instruments) to a thickness of >30 nm and imaged using a Zeiss Supra 55 VP-FESEM scanning electron microscope using an accelerating voltage of 5 kV.

For cryoSEM, samples were plunged into a liquid nitrogen slush at −190 °C and then transferred to a Gatan Alto 2500 cryo unit at −140 °C. The samples were etched at −95 °C for 10 min and then sputter coated with gold for 120 s at 10 mA. The samples were examined under a Zeiss Sigma VP-FESEM at −140 °C.

2.6. Mechanical testing of the printed blood vessels

Tensile measurements of a bioprinted vessel in the radial and circumferential directions were performed in a bath of PBS (pH 7.4) at room temperature. Samples were cut into strips and clamped to a uniaxial tensometer (CellScale UStretch, Waterloo, ON, Canada) equipped with a 4.4 N load cell. Samples were strained at 0.1 mm/s until a complete rupture was achieved. The tensometer recorded a tensile force at a frequency of 10 Hz. Prior to mechanical testing, the wall thickness of the vessel was determined using a microscope. Briefly, a printed construct was imaged using a 4× objective under an inverted phase contrast microscope (Nikon Eclipse Ti, Nikon, Tokyo, Japan). Tiled images were taken large enough to include both the whole length of the construct as well as the mandrel upon which it was cultured. The outer diameter of the rod and the construct were taken at 5 points, averaged, and used to calculate the average wall thickness. The sample dimensions were then used to convert recorded force and displacement data into average uniaxial engineering stress and strain. An estimation of the burst pressure of vascular constructs was calculated using the Barlow's equation.

$$P_{Burst} = \frac{2tS}{OD} \tag{1}$$

where S is a circumferential ultimate tensile strength (UTS) of the sample, t is the wall thickness, and the OD is the outer diameter of the sample.

The compliance (C) of the vascular constructs was estimated as suggested by Roeder et al. [70]:

$$C = \frac{1}{E_c}\frac{OD}{2t} \tag{2}$$

where E_c is a circumferential elastic modulus, t is the wall thickness, and OD is the outer diameter of the sample. Compliance was reported as %/mmHg.

The anisotropy index of the vascular construct was calculated as follows:

$$I = \frac{E_c}{E_z} \tag{3}$$

where E_c is an elastic modulus of the sample when stretched as a circumferential strip, whereas E_z is an elastic modulus of the sample when stretched as an axial strip along the length of the rod.

2.7. Histology

A 5-mm piece of the printed constructs were fixed in 4% (w/v) paraformaldehyde for 40 min, followed by a cryoprotective step in 30% (w/v) sucrose overnight. Samples were embedded in an optimal cutting temperature (OCT) medium, flash frozen using liquid nitrogen, and cut into 10-μm transverse slices. Slices were stained using either a hematoxylin and eosin procedure (H&E), a modified Verhoeff Van-Giesen procedure, or a Gömöri trichrome procedure.

2.8. Statistical analysis

All data are expressed as mean ± standard deviation. Statistical differences are determined with Student's *t*-test and differences are considered statistically significant at *p*-value of 0.033 or less.

Please cite this article as: S. Freeman, R. Ramos, P. Alexis Chando et al., A bioink blend for rotary 3D bioprinting tissue engineered small-diameter vascular constructs, Acta Biomaterialia, https://doi.org/10.1016/j.actbio.2019.06.052

3. Results

3.1. Development of a rotary bioprinter for 3D printing TEVGs

As shown in Fig. 1A, we developed a novel 3D rotary bioprinter for biofabricating TEVGs. The printer was controlled by an Arduino Mega 2560 microcontroller and all axes were stepper motor-driven. Vessel constructs were printed helically on a rotating polystyrene rod (Fig. 1B). The polystyrene rod can be readily fabricated or 3D printed to a desired diameter and length to meet individual patient's need. To print a vessel, we used a NEMA14-powered extrusion gantry that was designed to hold a different size of syringes such as a 1- or 3-mL syringe to extrude viscous bioinks for a layer-by-layer rotatory printing based on a predetermined architecture. The syringes were fitted with a 24G tapered tip (ID = 0.334 mm). The linear extrusion rates were typically 100 mm/min. Multiple heads can be configured for the printer if needed. Each head can be used to print different types of cells and bioinks. All vascular constructs were printed using a circumferential and axial motion at the same time.

To determine the volume of a bioink needed for printing, the following formula was adopted:

$$V_{extruded} = \pi L t (t + OD_{pipet}) \quad (4)$$

where L is the length of the construct, t is the wall thickness, and OD is the outer diameter of the polystyrene rod that served as a mandrel. We chose a polystyrene rod with a 4.9 mm OD that is in a range of small diameter vascular grafts (<6 mm). The initial thickness of the vessels was determined by the number of layers printed on the mandrel. However, the vessels were remodeled continuously by ECM secreted from cells during the vessel development. Thus, the final diameter of the vessels were determined by culture conditions designed to tissue engineer vascular grafts after printing. This rotary printing technology offers a new solution enabling low-cost and rapid vascular graft printing.

3.2. Development of a bioink for rotary tissue printing

Fibrinogen is a promising biomaterial for TEVGs [51,52,67]. It is, however, not printable as discussed above. To make it printable, we explored a new approach by blending it with gelatin to alter its rheological properties. As a thermoreversible biomaterial, the mixing of gelatin with fibrinogen will increase its elasticity after cooling. As the interlinking of its fiber network is caused by hydrogen bonding, it can undergo a transition from a solidified gel to a liquefied solution by rising the temperature from low such as 4 °C to high such as 25 °C. The blending of gelatin with fibrinogen bestows shear-thinning rheological properties needed for 3D bioprinting to the bioink. The printed vascular constructs can then be placed in a thrombin bath for crosslinking at room temperature. Once the fibrin network is formed, the whole constructs can be placed in an incubator at 37 °C to remove the gelatin, creating a porous structure favorable for cells to grow and organize into a tissue structure (Fig. 1C–F). We discovered that the heat treatment of gelatin remarkably affects the shear-thinning properties of the ink, which in turn influences the printability of fibrinogen for fabricating TEVGs.

3.2.1. Characterization of printability and shear-thinning properties of the blended gelatin-fibrinogen bioink

To determine the printability of the gelatin-fibrinogen blended bioink, we first investigated the printability of gelatin. We found that the heat treatment and concentration of gelatin are two key parameters determining the printability of gelatin. Heat-treatment has been used to modify the printability and the cell viability of gelatin-based bioinks [67]. We prepared a panel of different gelatin treated at 90 °C for various durations ranging from 1 h to 9 h. The heat-treated gelatins were helically printed to study the effect of heat treatment and concentration on the printability of the bioinks (Fig. 2A). We found that the longer the gelatin was heated, the less viscous it became. The increase in concentration of gelatin seemed to compensate this trend. A high concentration of gelatin tended to be stiffer, enabling it to hold its shape on the mandrel against the gravity during printing. Extended heating times produced a low concentration gelatin solution that was unable to gel and instead became a viscous solution that flowed off from the surface of the mandrel. We found that for a heat treatment of 1 h at 90 °C a concentration of 3.75% (w/v) or higher was needed in order to have an extrudable bioink that could maintain its shape during printing. Higher than 10% (w/v) resulted in bioinks that were too viscous and stiff to be extruded by the printer. It appears that gelatin becomes more printable when it is used at a low concentration and heated for a short period or at a high concentration and heated for a longer period.

To determine whether the blending of gelatin with fibrinogen affects its printability, we added 10 mg/mL fibrinogen to the gelatin and printed as described above. As shown in Fig. 2B, the mixing of fibrinogen with 1 h heat-treated gelatin did not seem to alter its printability significantly. SEM analysis of gelatin and gelatin-fibrinogen bioinks revealed similar pore structures of these two bioinks (Fig. 2C).

Next, we interrogated how heat treatment affected rheological properties of the bioink. We found that the dynamic viscosity and storage moduli of gelatin increased with an increase in gelatin concentration, but decreased with extended heat treatment (Fig. 3A & B). For longer heat treatment, the effect of gelatin concentration on viscosity and storage moduli became more profound for heat-treated gelatin. Characterization of bioink's shear-thinning property divulged a critical role of heat treatment in determining rheological properties of the gelatin-fibrinogen bioinks. As shown in Fig. 3C, gelatin and a gelatin-fibrinogen bioink possess a similar viscosity profiles, whereas fibrinogen is five-orders of magnitude less viscous than gelatin and four-orders of magnitude less viscous than the bioink blend under a shear force. These results highlighted the importance of viscosity as one of the primary rheological parameters for determining printability of a bioink. The blending of fibrinogen with gelatin did seem to alter shear-thinning property of the gelatin. In other words, the shear-thinning property of a gelatin-fibrinogen blended bioink is mainly dependent upon the gelatin's shear-thinning property.

SEM analysis of freeze-dried 10% (w/v) 1 h heat-treated gelatin or 5% 9 h treated gelatin did not reveal a porous structure. Instead, they showed a rough, scaly surface (Fig. 3D). In contrast, the 10% (w/v) 9 h heat-treated gelatin or 5% (w/v) 1 h heat-treated gelatin formed a porous structure. CryoSEM that is able to image gels in a higher state of hydration unveiled a trend of increasing gel density when concentration of gelatin increases for gelatin that were heated in a short period. Longer heat treatment rendered the microstructure of a low concentration gelatin that becomes less interconnected (Fig. 3E). The longer heat treatment of a high concentration gelatin appeared to make a gel much dense and lose its porous structure.

The inclusion of cells into the gelatin-fibrinogen bioinks also altered the printability of the bioink. We observed that the bioink became a viscous liquid instead of a gel after cells were added to the gelatin-fibrinogen hydrogel, reducing its printability, as shown in Fig. 4A, B. Fig. 4C shows visual images of bioinks containing different number of cells. Clearly, the more cells were added to the bioink, the more liquefied the bioink became. The addition of cells to the gelatin-fibrinogen bioink impairs the gelation of heat-treated gelatin. SEM revealed the disruption of microstructures of

Please cite this article as: S. Freeman, R. Ramos, P. Alexis Chando et al., A bioink blend for rotary 3D bioprinting tissue engineered small-diameter vascular constructs, Acta Biomaterialia, https://doi.org/10.1016/j.actbio.2019.06.052

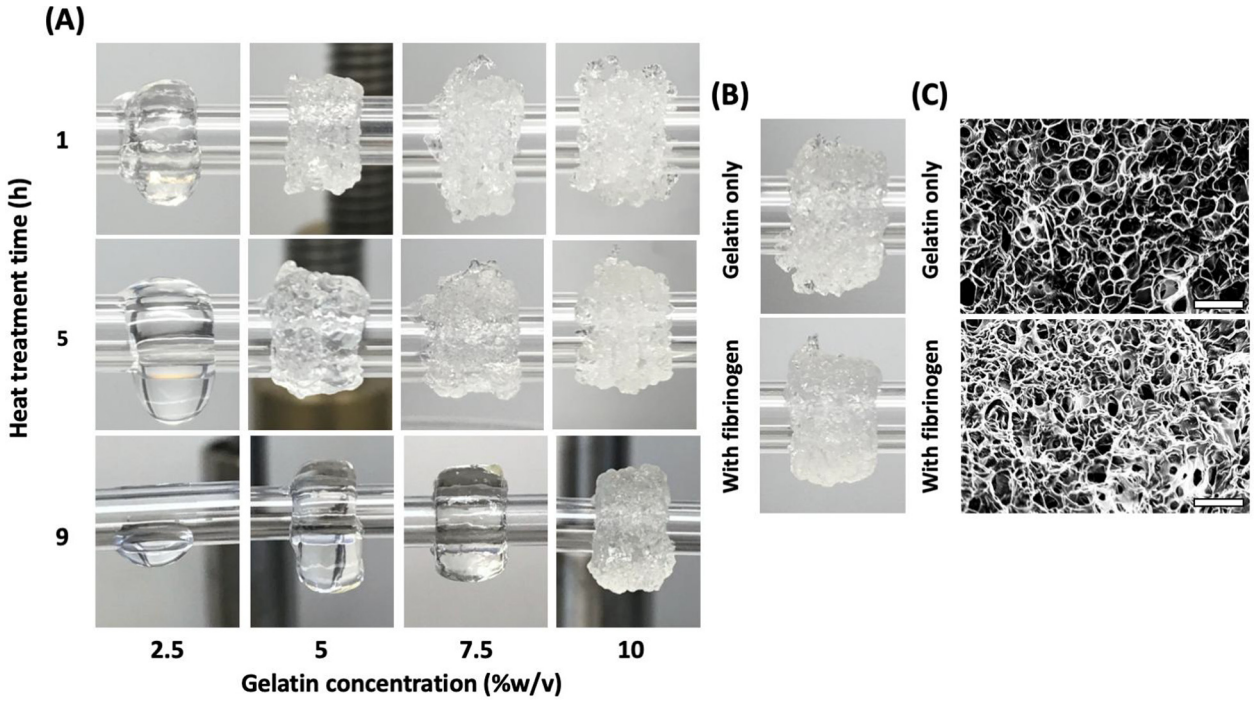

Fig. 2. Printability of gelatin-fibrinogen blended bioinks. (A) Helically printed gelatin constructs using different concentrations of heat-treated gelatin ranging from 2.5 to 10% (w/v). A 15%(w/v) gelatin was heated to 90 °C for 1, 5, and 9 h and then diluted into different concentrations for printing. Gelatin was chilled to 4 °C to gel and then placed at room temperature for at least 1 h before printing. (B) A comparison between 1 h heat-treated gelatin (7.5%(w/v)) and gelatin (7.5%w/v)-fibrinogen (10 mg/mL) blended bioink. (C) SEM micrographs of 1 h heat-treated gelatin (5%(w/v) and gelatin (5%w/v)-fibrinogen (10 mg/mL) blended bioink. Scale bar: 10 μm.

a gelatin-fibrinogen bioink due to its mixing with cells (Fig. 4D). These results suggested that the printed constructs tend to deform and flow off from the rod of the printer when the gelatin is heat-treated too long, or the bioink entails a high density of cells. A printable bioink should allow for printing a construct that maintains its shape on the mandrel against the gravity during printing. To conclude, there are three factors influencing the rheological properties of the gelatin-fibrinogen bioink blend, i.e. the concentration and heat treatment of gelatin as well as the density of cells that are mixed with the bioink.

Another factor that we investigated is the ability of a bioink to maintain a high cell survival rate during and after printing. We performed an ethidium homodimer-1 staining to quantify the cell death after printing. Ethidium homodimer-1 is a cell impermeant fluorescent dye that binds to DNA of cells with damaged or compromised membranes. As shown in Fig. 4E, F, cell viability dropped in a high concentration (>8.75% (w/v)) and shorter-time heat-treated gelatin fibrinogen bioink blend. The cell viability was 84.7 ± 0.5% when 5% 1 h heat-treated gelatin was used for preparing a gelatin-fibrinogen bioink blend that contained 1×10^6 cells/mL. It dropped to 61.6 ± 2.6% when printing with 10% (w/v) 1 h heat-treated gelatin blended cell-laden gelatin-fibrinogen bioink. The same trend was observed when printing with 3×10^6 cells/mL-laden bioinks. Cell viability was maintained higher than 80% in all tested conditions, suggesting that the cell viability during and after printing might not be a great concern when a gelatin-fibrinogen bioink blend is used for 3D rotary printing.

3.3. Effect of thrombin concentration on crosslinking of cell-laden bioinks

Next, we characterized the effect of thrombin concentrations on vascular printing. Vascular constructs were printed using 7.5%(w/v) 1 h heat-treated gelatin mixed with 10 mg/mL fibrinogen and 3×10^6 cells/mL. The printed constructs were incubated in various concentrations of bovine thrombin (1, 5, 10, and 20 U/mL) for 1 h at room temperature. HEPES was added to the cell culture medium to protect against pH changes while fibrin clotting occurred. After crosslinking, we placed the constructs in a CO_2 incubator overnight and examined the next day. As mentioned above, gelatin leaked out from the crosslinked fibrinogen network, generating porous scaffolds for cells to grow and assemble into a vessel structure. As shown in Fig. 5A, we found that more uniform vascular constructs could be formed when a low concentration of thrombin was employed for crosslinking. A concentration higher than 20 U/mL led to the formation of lumps on the underside of the conduits, presumably due in part to the gravity. The formation of a fibrinogen network was detected when mixing gelatin with rhodamine-conjugated fibrinogen. We observed interconnected fibrin networks formed after crosslinking (Fig. 5B). In the absence of cells, we observed the formation of porous structures with the fibrin arranged in a honeycomb-like structure. In the presence of cells, the fibrin fiber networks became more condensed around and in between cells.

3.4. Tissue engineering of printed vascular constructs

Finally, we evaluated whether the printed vascular constructs could develop into TEVGs. We prepared a bioink blend entailing 3×10^6 cells/mL, 10 mg/mL fibrinogen, and 7.5% (w/v) 1 h heat-treated gelatin for printing a vascular construct on a rotary bioprinter. To observe the development of TEVGs after printing, we used GFP-expressing HDF-n cells that allow for visualizing the changing of cellular morphology within the printed the vascular constructs during cultures. The fibroblast cells became more elongated at day 5 (Fig. 6A). These cells exhibited different morphology in the different regions of the vessel. Fibroblasts near the vessel surface were circumferentially aligned as shown in Region I (Fig. 6A), whereas cells in the inner layer (luminal side) of the ves-

Please cite this article as: S. Freeman, R. Ramos, P. Alexis Chando et al., A bioink blend for rotary 3D bioprinting tissue engineered small-diameter vascular constructs, Acta Biomaterialia, https://doi.org/10.1016/j.actbio.2019.06.052

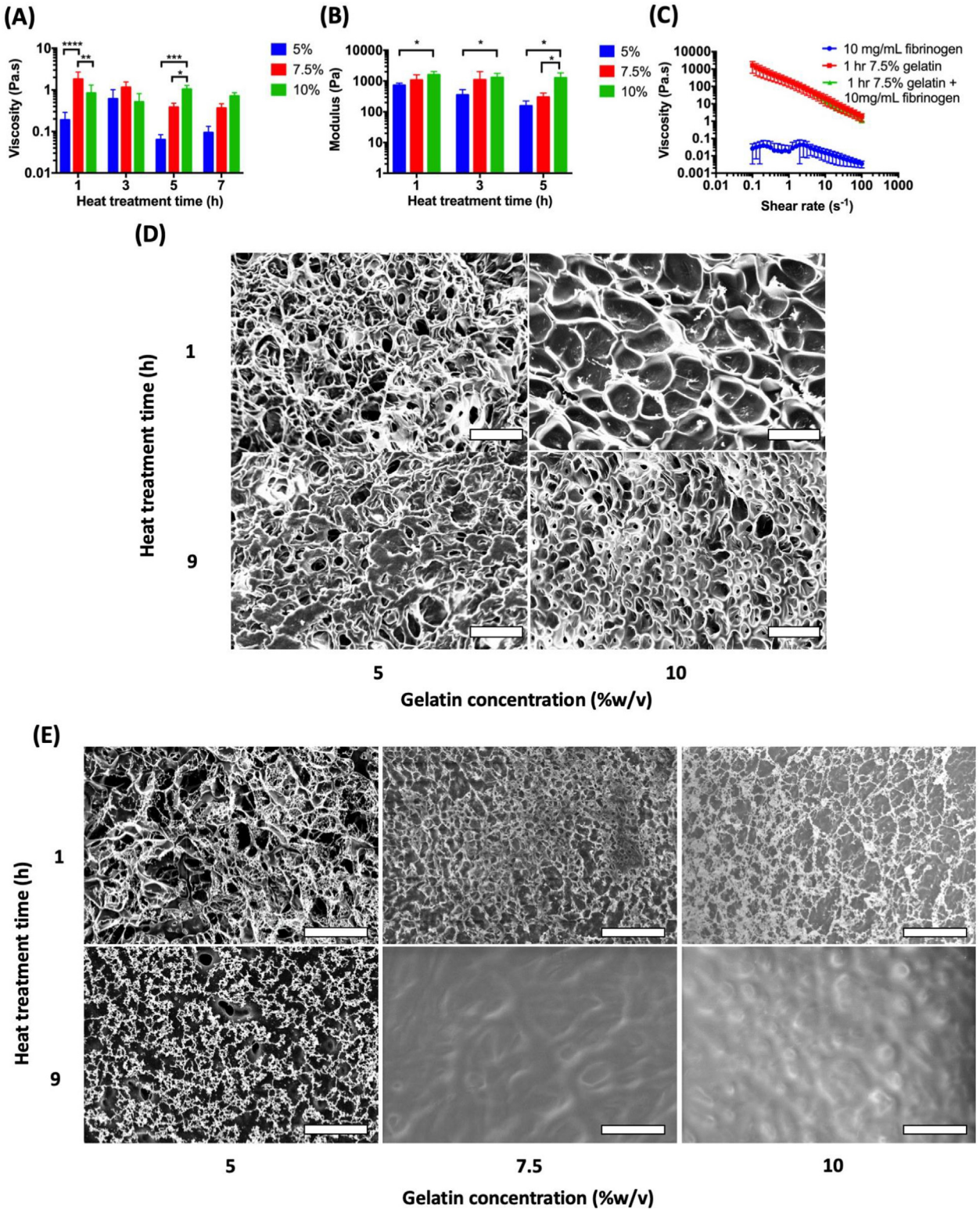

Fig. 3. Effect of heat treatment on gelatin's rheological and microstructural properties. Effect of heat treatment on (A) the viscosity and (B) the shear storage moduli of gelatin. Gelatin was heated at 90 °C for various times (1–7 h) and then diluted to 5, 7.5%, and 10%. The viscosity was measured at a shear rate of 100 s^{-1}, whereas the storage modulus was measured at an oscillatory frequency of 0.1 Hz. Data are presented as mean ± S.D. *, $p < 0.03$; **, $p < 0.002$; ***, $p < 0.0002$; and ****, $p < 0.0001$. (C) shear-thinning properties of the bioinks. (D) SEM of gelatin-fibrinogen bioink. Scale bar: 10 μm. (E) Cryo-SEM of gelatin-fibrinogen bioinks. Scale bar: 10 μm.

sel (Region II) became more spindle-like (Fig. 6C). Histological staining of the vessels at day 3, day 24, and day 45 revealed increased collagen deposition detected by Gömöri trichome (blue) and Verhoeff Van Gieson (VVG) (red) staining (Fig. 6D, E). However, hematoxylin and eosin (H&E) staining did not reveal any noticeable change of collagen in the vessel over the time, suggesting H&E might not be a good choice for detecting collagen in fibrinogen printed vessel constructs. The heavy purple-pink background

Please cite this article as: S. Freeman, R. Ramos, P. Alexis Chando et al., A bioink blend for rotary 3D bioprinting tissue engineered small-diameter vascular constructs, Acta Biomaterialia, https://doi.org/10.1016/j.actbio.2019.06.052

(A) 1 x 10^6 cells per mL

Heat treatment time (h)

Gelatin concentration in bioink %(w/v)	1	3	5	7	9
5	87.80	81.92	85.78	90.76	91.72
6.25	86.95	81.94	81.33	89.45	91.70
7.5	83.76	83.24	80.72	89.66	90.35
8.75	77.49	80.71	80.04	89.49	89.61
10	69.34	77.38	84.48	90.51	89.85

Not printable

Printable

(B) 3 x 10^6 cells per mL

Heat treatment time (h)

Gelatin concentration in bioink %(w/v)	1	3	5	7	9
5	93.44	91.66	91.82	93.70	94.46
6.25	93.17	91.49	91.06	93.59	93.51
7.5	91.38	91.75	92.01	92.97	92.93
8.75	89.43	88.67	91.34	92.45	93.24
10	84.96	87.40	91.83	92.00	92.82

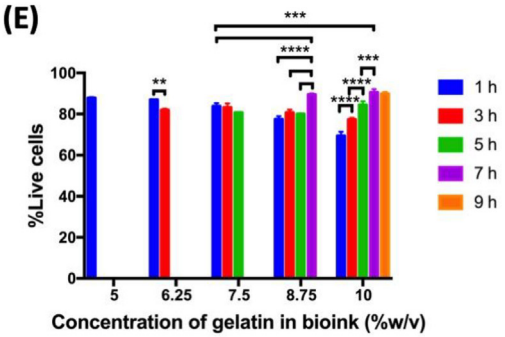

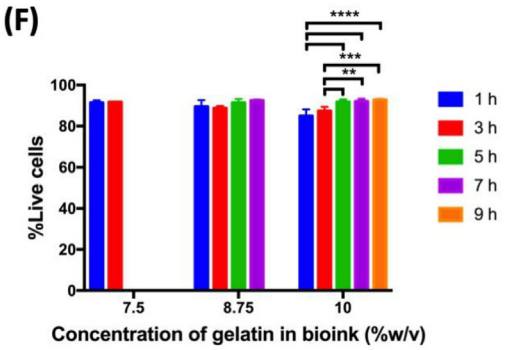

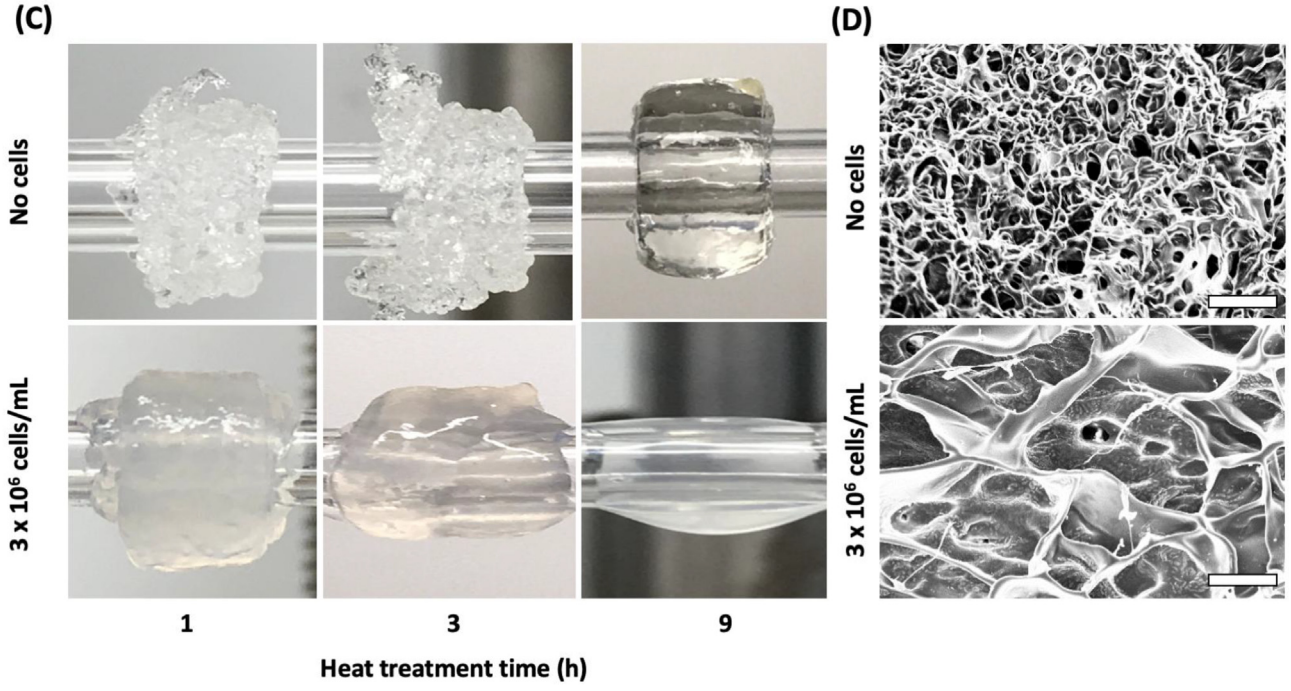

Fig. 4. Effect of heat treatment of gelatin on cell viability during 3D rotary printing. (A) 1 × 10^6 or (B) 3 × 10^6 cells/mL neonatal human dermal fibroblasts (HDF-n) were mixed with the gelatin-fibrinogen bioink for vascular 3D rotary printing. The gelatin was heat treated at 90 °C before used for preparing the bioinks. Red region indicated poor printability of the cell-laden bioinks, while the green regions indicated conditions that held. Average percentage of live cells detected by ethidium homodimer staining are shown in the table. (C) The appearance of tubular tissue constructs printed using cell-laden bioinks prepared using 10 mg/mL of fibrinogen and 7.5% (w/v) heat-treated gelatin. (D) SEM micrographs of the 5% (w/v) 1 h heat-treated gelatin + 10 mg/mL fibrinogen. Scale bar: 10 μm. Percentage of live cells in gelatin-fibrinogen bioinks containing (E) 1 × 10^6 cells/mL or (F) 3 × 10^6 cells/mL. Data are presented as mean ± S.D. *, $p < 0.033$; **, $p < 0.0021$; ***, $p < 0.0002$; and ****, $p < 0.0001$. (For interpretation of the references to colour in this figure legend, the reader is referred to the web version of this article.)

observed in H&E stained at day 24 was due to a poor washing of the eosin dye from the glass slide.

Interestingly, we observed a significant volumetric reduction of the vascular constructs in the cultures (Fig. 6F, G), with the greatest change occurring in the beginning of the culture (*data not shown*), due in part to the washing out of gelatin from the printed vessel constructs and the growth of fibroblast cells that tightened the matrix. The length of the vessel constructs decreased at a similar rate. It does not seem that the printing cell density affects length reduction in the cultures. It was about 0.908 ± 0.155 when printing with 1×10^6 cells/mL. It was 1.03 ± 0.073 mm/day for 3×10^6 cells/mL. However, the thickness of the vessel constructs decreased rapidly in the first 3 days and then became plateau afterwards. However, the printing cell density also influences the thickness

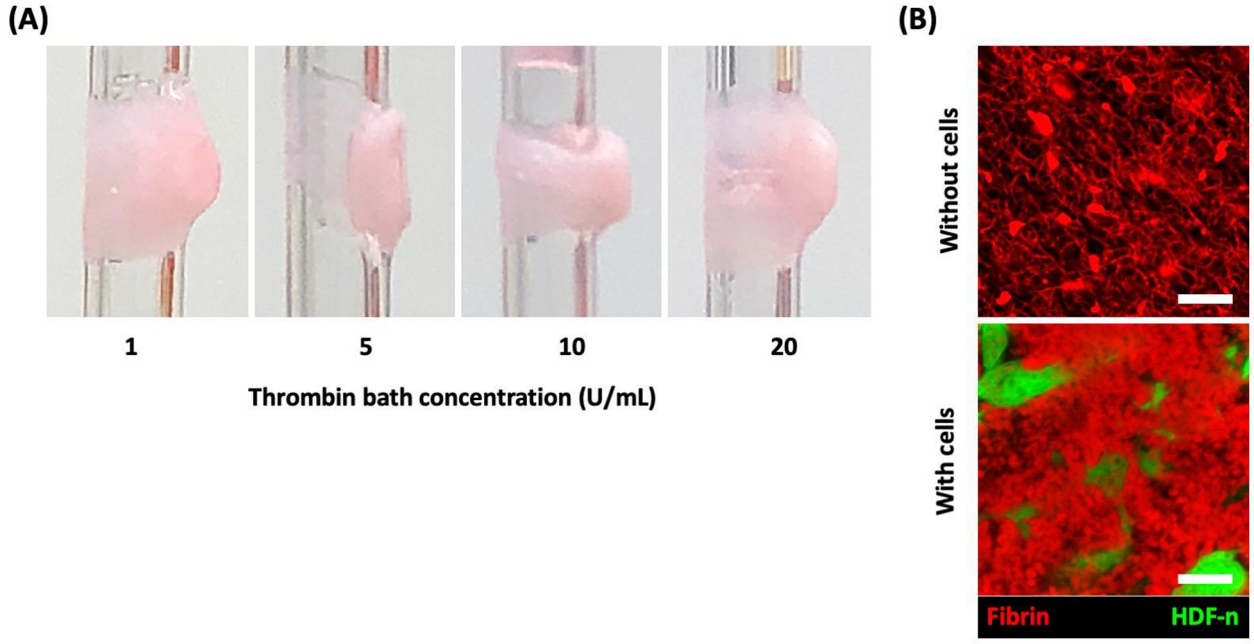

Fig. 5. Effect of thrombin concentration on cell-laden bioink crosslink after printing. (A) Effect of thrombin concentration on the crosslinking of cell-laden bioinks. The cell-laden bioink was prepared by mixing 7.5% (w/v) 1 h heat-treated gelatin with 10 mg/mL fibrinogen and 1×10^6 cells. (B) Fluorescence micrographs of fibrin networks formed with and without cells at 24 h after printing. 3×10^6 cells/mL was printed along with the bioink. Scale bar: 10 μm. Fibrin was labeled with Rhodamine (red). Green, GFP-expressing HDF-n cells. (For interpretation of the references to colour in this figure legend, the reader is referred to the web version of this article.)

reduction considerably. The thickness of the vessel at day 7 was 305.630 ± 49.758 μm when printing with 1×10^6 cells/mL, whereas it drops below 125.824 ± 50.872 μm when printing with 3×10^6 cells/mL.

We grew the constructs up to two months and tracked the changes in mechanical properties in the circumferential and axial directions. Elastic modulus, burst pressure, and ultimate tensile strength of the vessels increased over the time, whereas a compliance of the vessel decreased with an increase in the circumferential stiffness and wall thickness reduction. The elastic moduli for the circumferential and axial directions of the tissue equalized over the time. As shown in Fig. 6H, I, the circumferential elastic modulus and ultimate tensile strength increased significantly with the culture. An analysis of the axial mechanical properties and the anisotropy index revealed that the circumferential elastic modulus started proportionally higher than the axial elastic modulus at the beginning of culture but the axial elastic modulus slowly increased over the time to be similar in magnitude (Fig. 6J). Interestingly, we observed a decrease in compliance of the vascular constructs in the culture, which could be associated with an increase in a circumferential stiffness and decrease in vessel thickness (Fig. 6K). The estimated burst pressure of the vessel constructs increased in the culture, with one of the samples reaching 2.4 MPa. This value corresponds to an estimated burst pressure of 1110 mm Hg using the Barlow's formula for estimating a burst pressure from the UTS (Fig. 6L). This is promising, as it is about 52% of the burst pressure of a human saphenous vein [2] and 35% of the burst pressure of an internal thoracic artery (ITA) (3196 ± 1264 mmHg) [32].

4. Discussion

Here, we demonstrated a novel 3D bioprinting approach on a rotating cylindrical surface for the fabrication of vascular constructs. 3D printing offers a free-form fabrication method and control of construct dimensions. Although 3D bioprinters using Cartesian coordinates have been used previously for creating blood vessels [38], the use of a rotating mandrel complements the fabrication of a tissue with cylindrical geometries and avoids the need for the use of support materials if very long vessels needs to be printed.

The fibrinogen is able to crosslink using thrombin, making it an ideal biomaterial for fabricating a soft tissue such as a vessel construct. However, its viscosity and stiffness is insufficient for bioprinting using a 3D rotary bioprinter due to its lacking of ability to hold its shape on the mandrel against gravity during the printing. We showed that the mixing of fibrinogen with more viscous gelatin gel bestows a desired shear-thinning property to the fibrinogen, making it printable for fabricating vessel constructs. We discovered that the printability of the blended bioink is tunable by pre-heat treatment of gelatin. Heating is considered to cause a decrease in molecular weight of the gelatin [62]. It has been reported more recently in studies of extracting gelatin from animal sources [71–73]. Sinthusamran et al. reported a decrease in gelatin gel strength with a longer extraction time or a higher extraction temperature [71], which parallels the trend that we observed on changes in shear storage modulus of gelatin over longer heat treatment. We demonstrated that the control of the shortening of molecular weights of gelatin through heat treatment can be used to tune the printability of the gelatin-fibrinogen bioink blend for vascular printing.

To crosslink the blended bioink, the thrombin must be diffused into the printed hydrogel. It is interesting that a lower concentration of thrombin yielded the printing of more uniform vessel constructs. We speculate that a higher concentration thrombin impairs its own diffusion into the hydrogel, as it rapidly crosslinks the outermost layers of the fibrin matrix, thereby reducing its permeability into the subsequent layers. A lower concentration of thrombin permits a slower reaction rate, which allows more thrombin to be diffused into the hydrogel before the outside layers become too dense.

We noticed a rapid and substantial shrinking of the printed vessel constructs at the beginning of the culture. The shrinking slowed

Please cite this article as: S. Freeman, R. Ramos, P. Alexis Chando et al., A bioink blend for rotary 3D bioprinting tissue engineered small-diameter vascular constructs, Acta Biomaterialia, https://doi.org/10.1016/j.actbio.2019.06.052

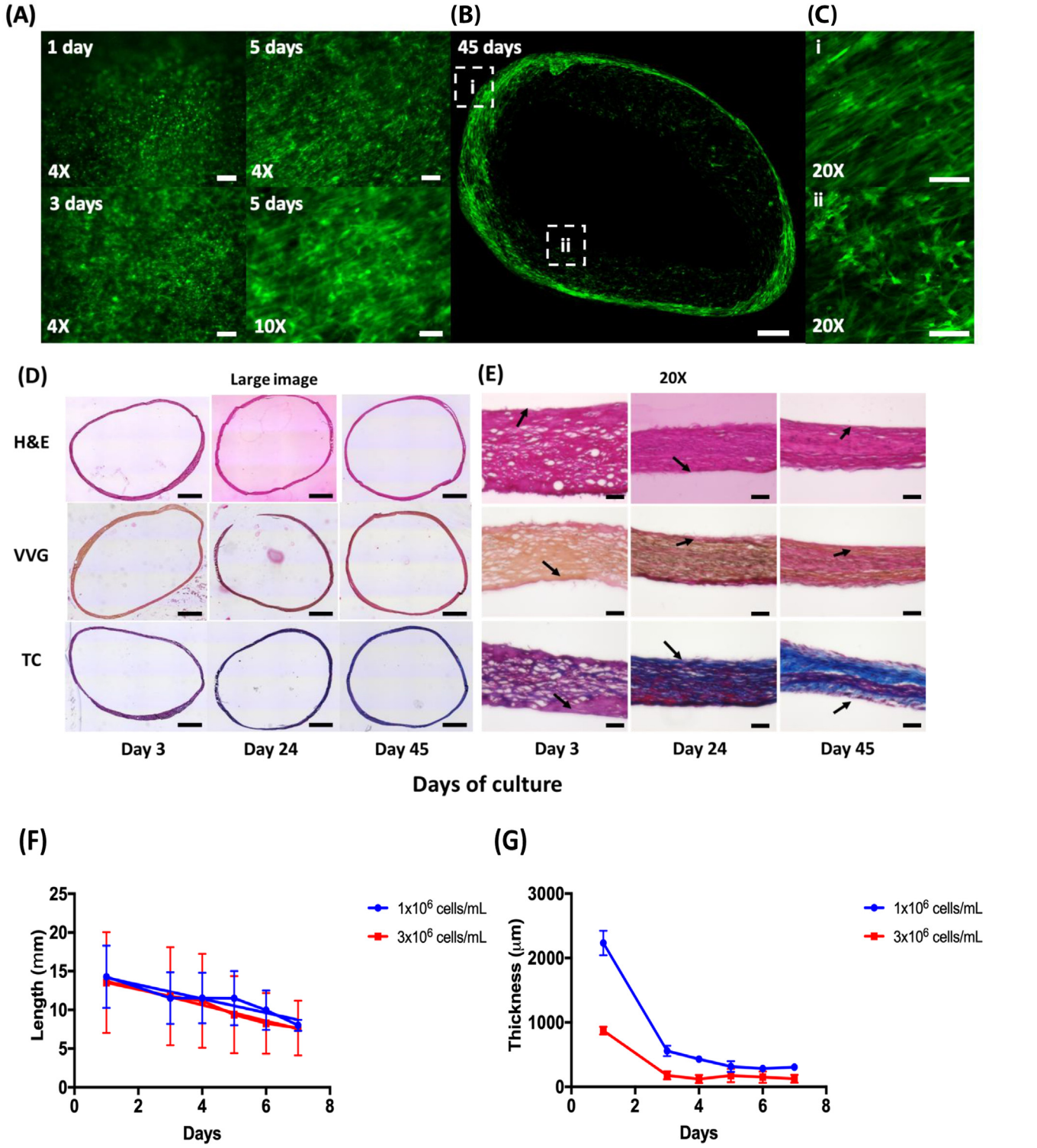

Fig. 6. The development of tissue engineered vascular constructs through 3D rotary bioprinting. (A) Fluorescence micrographs of GFP-HDF-n grown within the printed fibrinogen vascular constructs at day 1, 3, and 5. Scale bar: 200 μm (4×) and 100 μm (10×). (B) A vessel structure formed at Day 45. (C) Multiphoton confocal micrographs of cells grown in different regions of the vessel. Region I: outer layer of the vessel. Region II: inner layer of the vessel. Scale bar: 100 μm. Histological section (D) and cross-section (E) images of vessels examined by hematoxylin & eosin (H&E), Verhoeff-Van Gieson (VVG), and Gömöri trichome (TC) staining at day 3, 24, and 45. Scale bar: 1 mm (D) and 50 μm (E). Arrows indicate a lumenal side of the vessel. (F) A time course of vessel condensed in length. (G) A time course of vessel condensed in thickness. (H) Circumferential elastic modulus, (I) circumferential ultimate tensile strength (UTS), (J) anisotropy index, (K) compliance, and (L) burst pressure of vascular constructs.

down after one or two days of culture. The removal of gelatin from the fibrin network might contribute to the rapid and substantial condensing of the vessel constructs at the beginning of the culture. The subsequent shrinking might be due to the contraction of fibroblast cells when they grow and become denser within the scaffold matrix. Other groups working on fibrin-based TEVGs have reported similar reduction in graft dimensions during the culture. Syedain et al. studied the importance of axial shortening for

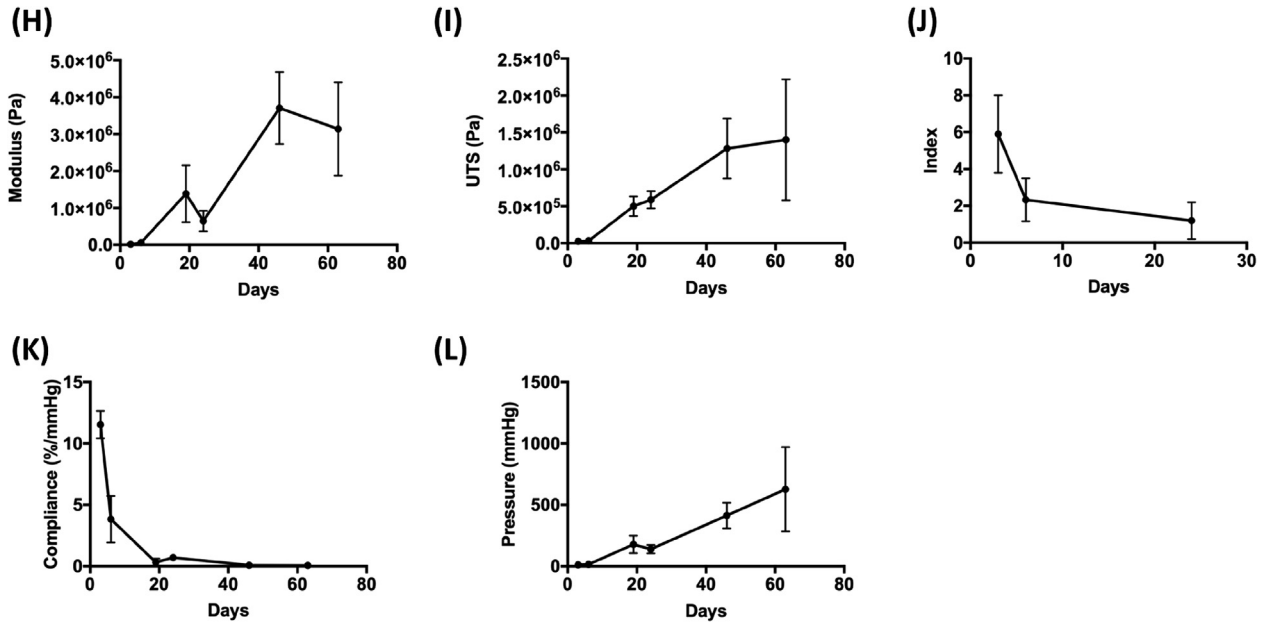

Fig. 6 (*continued*)

achieving anisotropy values closer to a target native ovine femoral artery (~3.3), and for improving circumferential elastic modulus and both circumferential and axial UTS values [18]. Their study using polarized light to track collagen fiber alignment shed light on our observations of mechanical anisotropy, suggesting that our constructs initially had very high circumferential fiber alignment due to the helical printing method used. Cell traction forces within the construct tend to align fibers axially, but axial shortening maintains the balance in favor of circumferential strength and stiffness.

Although a lower concentration of thrombin leads to the printing of more uniform vascular grafts, a noticeable sag on the underside of the constructs was still observed. This might explain why the whole vessel tended to have thicker walls on bottom side of the construct versus the top, as revealed by cross-sectioning staining. We observed differences in tissue uniformity even within constructs printed under the same condition. This may explain a high variation noticed in the mechanical values of the grafts through the long-term culture, as well as small patches of the tissue that did not undergo ECM remodeling, as can be seen in the 20× magnification of the 45-day old construct stained with Gömöri trichrome. We have already begun improving the biofabrication protocol to include thrombin in the bioink in addition to the thrombin bath, and it has shown promise for improving tissue distribution and decreasing the variation. Notwithstanding, the printed constructs presented here were able to behave similar to other fibrin-based TEVGs, giving validity to the bioprinting approach for producing clinically relevant tissue engineered products.

While we were focusing on bioink formulation for rotary bioprinting in this study, the augment of these studies will enable the printing of triple layered vessel grafts by depositing fibroblast cells, smooth muscle cells, and endothelial cells layer by layer to compartmentalize collagenous matrix, elastic fibers, smooth muscle layers, and endothelium using the 3D rotary bioprinter developed in our lab. This will overcome technological difficulties in printing such vascular structures when cell sheet or casting technologies are used for fabrication, as discussed above. It offers a solution to biomanufacture clinically relevant vascular grafts for CVD treatment.

5. Conclusion

We developed a novel bioink and rotary bioprinting for biofabricating customized and personalized vessel grafts. Analysis of different bioink formulations revealed a complexity of biomaterial printability, cell viability, and tissue formation during and after 3D bioprinting. We showed that the neonatal human dermal fibroblasts can be printed at high concentrations. Furthermore, the secrete ECMs remodel the vessel to a desired burst pressure. In particular, we observed the increase in collagen deposition from the cells during the cultures, leading to an increase in mechanical stiffness and strength over time.

Acknowledgements

This work was partially supported by NSF CBET 0756455, CBET 1445387, EEC 1757846, and CBET 1531944. The authors wish to thank Dr. Eric Finkelstein, Edgardo Velazquez, and Ioannis Miltiadis Stravrinoudis from Syracuse Biomaterials Institute for their time and expertise related to rheological testing as well as Dr. Guy German and Dr. Liu Xue for their training and use of their tensometer. We would also like to acknowledge Dr. Siyang Zheng and Yiqiu Xia from Pennsylvania State University and John Cantolina from the Huck Institutes for their assistance with scanning electron cryomicroscopy.

Appendix A. Supplementary data

Supplementary data to this article can be found online at https://doi.org/10.1016/j.actbio.2019.06.052.

References

[1] Cardiovascular diseases (CVDs), (2017). https://www.who.int/en/news-room/fact-sheets/detail/cardiovascular-diseases-(cvds) (accessed 20.03.19).
[2] G.L. Buchanan, A. Chieffo, E. Meliga, R. Mehran, S.-J. Park, Y. Onuma, P. Capranzano, M. Valgimigli, I. Narbute, R.R. Makkar, I.F. Palacios, Y.-H. Kim, P.P. Buszman, T. Chakravarty, I. Sheiban, C. Naber, R. Margey, A. Agnihotri, S. Marra, D. Capodanno, V. Allgar, M.B. Leon, J.W. Moses, J. Fajadet, T. Lefevre, M.-C. Morice, A. Erglis, C. Tamburino, O. Alfieri, P.W. Serruys, A. Colombo,

Comparison of percutaneous coronary intervention (with drug-eluting stents) versus coronary artery bypass grafting in women with severe narrowing of the left main coronary artery (from the Women-Drug-Eluting stent for LefT main coronary Artery disease Reg, Am. J. Cardiol. 113 (2014) 1348–1355, https://doi.org/10.1016/j.amjcard.2014.01.409.

[3] F.W. Mohr, M.-C. Morice, A.P. Kappetein, T.E. Feldman, E. Ståhle, A. Colombo, M. J. Mack, D.R. Holmes, M. Morel, N. Van Dyck, V.M. Houle, K.D. Dawkins, P.W. Serruys, Coronary artery bypass graft surgery versus percutaneous coronary intervention in patients with three-vessel disease and left main coronary disease: 5-year follow-up of the randomised, clinical SYNTAX trial, Lancet (London, England) 381 (2013) 629–638, https://doi.org/10.1016/S0140-6736(13)60141-5.

[4] P.W. Serruys, M.-C. Morice, A.P. Kappetein, A. Colombo, D.R. Holmes, M.J. Mack, E. Ståhle, T.E. Feldman, M. van den Brand, E.J. Bass, N. Van Dyck, K. Leadley, K.D. Dawkins, F.W. Mohr, SYNTAX Investigators, Percutaneous coronary intervention versus coronary-artery bypass grafting for severe coronary artery disease, N. Engl. J. Med. 360 (2009) 961–972, https://doi.org/10.1056/NEJMoa0804626.

[5] A.E. Rodriguez, H. Pavlovsky, J.F. Del Pozo, Understanding the outcome of randomized trials with drug-eluting stents and coronary artery bypass graft in patients with multivessel disease: a review of a 25-year journey, Clin. Med. Insights Cardiol. 10 (2016) 195–199, https://doi.org/10.4137/CMC.S40645.

[6] S. Pashneh-Tala, S. MacNeil, F. Claeyssens, The tissue-engineered vascular graft-past, present, and future, Tissue Eng. B Rev. 22 (2016) 68–100, https://doi.org/10.1089/ten.teb.2015.0100.

[7] H.-Y. Mi, X. Jing, E. Yu, X. Wang, Q. Li, L.-S. Turng, Manipulating the structure and mechanical properties of thermoplastic polyurethane/polycaprolactone hybrid small diameter vascular scaffolds fabricated via electrospinning using an assembled rotating collector, J. Mech. Behav. Biomed. Mater. 78 (2018) 433–441, https://doi.org/10.1016/j.jmbbm.2017.11.046.

[8] R. Johnson, Y. Ding, N. Nagiah, E. Monnet, W. Tan, Coaxially-structured fibres with tailored material properties for vascular graft implant, Mater. Sci. Eng. C Mater. Biol. Appl. 97 (2019) 1–11, https://doi.org/10.1016/j.msec.2018.11.036.

[9] H.-Y. Mi, X. Jing, J. McNulty, M.R. Salick, X.-F. Peng, L.-S. Turng, Approaches to fabricating multiple-layered vascular scaffolds using hybrid electrospinning and thermally induced phase separation methods, Ind. Eng. Chem. Res. 55 (2016) 882–892, https://doi.org/10.1021/acs.iecr.5b03462.

[10] W. Wang, W. Nie, D. Liu, H. Du, X. Zhou, L. Chen, H. Wang, X. Mo, L. Li, C. He, Macroporous nanofibrous vascular scaffold with improved biodegradability and smooth muscle cells infiltration prepared by dual phase separation technique, Int. J. Nanomed. 13 (2018) 7003–7018, https://doi.org/10.2147/IJN.S183463.

[11] M. Peck, D. Gebhart, N. Dusserre, T.N. McAllister, N. L'Heureux, The evolution of vascular tissue engineering and current state of the art, Cells Tissues Organs. 195 (2012) 144–158, https://doi.org/10.1159/000331406.

[12] G. De Visscher, L. Mesure, B. Meuris, A. Ivanova, W. Flameng, Improved endothelialization and reduced thrombosis by coating a synthetic vascular graft with fibronectin and stem cell homing factor SDF-1α, Acta Biomater. 8 (2012) 1330–1338, https://doi.org/10.1016/j.actbio.2011.09.016.

[13] M.R. de Vries, K.H. Simons, J.W. Jukema, J. Braun, P.H.A. Quax, Vein graft failure: from pathophysiology to clinical outcomes, Nat. Rev. Cardiol. 13 (2016) 451–470, https://doi.org/10.1038/nrcardio.2016.76.

[14] L.V. Thomas, V. Lekshmi, P.D. Nair, Tissue engineered vascular grafts — Preclinical aspects, Int. J. Cardiol. 167 (2013) 1091–1100, https://doi.org/10.1016/j.ijcard.2012.09.069.

[15] Y. Zhang, X.S. Li, A.G. Guex, S.S. Liu, E. Müller, R.I. Malini, H.J. Zhao, M. Rottmar, K. Maniura-Weber, R.M. Rossi, F. Spano, A compliant and biomimetic three-layered vascular graft for small blood vessels, Biofabrication 9 (2017) 025010, https://doi.org/10.1088/1758-5090/aa6bae.

[16] N. L'Heureux, L. Germain, R. Labbé, F.A. Auger, In vitro construction of a human blood vessel from cultured vascular cells: a morphologic study, J. Vasc. Surg. 17 (1993) 499–509, https://doi.org/10.1016/0741-5214(93)90150-K.

[17] N. L'Heureux, S. Pâquet, R. Labbé, L. Germain, F.A. Auger, A completely biological tissue-engineered human blood vessel, FASEB J. 12 (1998) 47–56. https://doi.org/0892-6638/97/0012-0047.

[18] Z.H. Syedain, L.A. Meier, J.W. Bjork, A. Lee, R.T. Tranquillo, Implantable arterial grafts from human fibroblasts and fibrin using a multi-graft pulsed flow-stretch bioreactor with noninvasive strength monitoring, Biomaterials 32 (2011) 714–722, https://doi.org/10.1016/j.biomaterials.2010.09.019.

[19] K.T. Morin, A.O. Smith, G.E. Davis, R.T. Tranquillo, Aligned human microvessels formed in 3D fibrin gel by constraint of gel contraction, Microvasc. Res. 90 (2013) 12–22, https://doi.org/10.1016/j.mvr.2013.07.010.

[20] A.K. Ranjan, U. Kumar, A.A. Hardikar, P. Poddar, P.D. Nair, A.A. Hardikar, Human blood vessel-derived endothelial progenitors for endothelialization of small diameter vascular prosthesis, PLoS One 4 (2009) e7718, https://doi.org/10.1371/journal.pone.0007718.

[21] S.K. Norouzi, A. Shamloo, Bilayered heparinized vascular graft fabricated by combining electrospinning and freeze drying methods, Mater. Sci. Eng. C Mater. Biol. Appl. 94 (2019) 1067–1076, https://doi.org/10.1016/j.msec.2018.10.016.

[22] S.C. Schutte, Z. Chen, K.G.M. Brockbank, R.M. Nerem, Cyclic strain improves strength and function of a collagen-based tissue-engineered vascular media, Tissue Eng. A 16 (2010) 3149–3157, https://doi.org/10.1089/ten.TEA.2010.0009.

[23] M. Achilli, D. Mantovani, Tailoring mechanical properties of collagen-based scaffolds for vascular tissue engineering: the effects of pH, temperature and ionic strength on gelation, Polymers (Basel) 2 (2010) 664–680, https://doi.org/10.3390/polym2040664.

[24] C.L. Cummings, D. Gawlitta, R.M. Nerem, J.P. Stegemann, Properties of engineered vascular constructs made from collagen, fibrin, and collagen-fibrin mixtures, Biomaterials 25 (2004) 3699–3706, https://doi.org/10.1016/j.biomaterials.2003.10.073.

[25] J.D. Berglund, R.M. Nerem, A. Sambanis, Incorporation of intact elastin scaffolds in tissue-engineered collagen-based vascular grafts, Tissue Eng. 10 (2004) 1526–1535, https://doi.org/10.1089/ten.2004.10.1526.

[26] M.J.W. Koens, K.A. Faraj, R.G. Wismans, J.A. van der Vliet, A.G. Krasznai, V.M.J.I. Cuijpers, J.A. Jansen, W.F. Daamen, T.H. van Kuppevelt, Controlled fabrication of triple layered and molecularly defined collagen/elastin vascular grafts resembling the native blood vessel, Acta Biomater. 6 (2010) 4666–4674, https://doi.org/10.1016/j.actbio.2010.06.038.

[27] M.J.W. Koens, A.G. Krasznai, A.E.J. Hanssen, T. Hendriks, R. Praster, W.F. Daamen, J.A. van der Vliet, T.H. van Kuppevelt, Vascular replacement using a layered elastin-collagen vascular graft in a porcine model: one week patency versus one month occlusion, Organogenesis 11 (2015) 105–121, https://doi.org/10.1080/15476278.2015.1038448.

[28] V.A. Kumar, J.M. Caves, C.A. Haller, E. Dai, L. Liu, S. Grainger, E.L. Chaikof, Acellular vascular grafts generated from collagen and elastin analogs, Acta Biomater. 9 (2013) 8067–8074, https://doi.org/10.1016/j.actbio.2013.05.024.

[29] K.T. Morin, J.L. Dries-Devlin, R.T. Tranquillo, Engineered microvessels with strong alignment and high lumen density via cell-induced fibrin gel compaction and interstitial flow, Tissue Eng. A 20 (2014) 553–565, https://doi.org/10.1089/ten.TEA.2013.0262.

[30] E.D. Grassl, T.R. Oegema, R.T. Tranquillo, Fibrin as an alternative biopolymer to type-I collagen for the fabrication of a media equivalent, J. Biomed. Mater. Res. 60 (2002) 607–612. http://www.ncbi.nlm.nih.gov/pubmed/11948519.

[31] L.A. Meier, Z.H. Syedain, M.T. Lahti, S.S. Johnson, M.H. Chen, R.P. Hebbel, R.T. Tranquillo, Blood outgrowth endothelial cells alter remodeling of completely biological engineered grafts implanted into the sheep femoral artery, J. Cardiovasc. Transl. Res. 7 (2014) 242–249, https://doi.org/10.1007/s12265-013-9539-z.

[32] L. Yao, D.D. Swartz, S.F. Gugino, J.A. Russell, S.T. Andreadis, Fibrin-based tissue-engineered blood vessels: differential effects of biomaterial and culture parameters on mechanical strength and vascular reactivity, Tissue Eng. 11 (2005) 991–1003, https://doi.org/10.1089/ten.2005.11.991.

[33] L. Yao, J. Liu, S.T. Andreadis, Composite fibrin scaffolds increase mechanical strength and preserve contractility of tissue engineered blood vessels, Pharm. Res. 25 (2008) 1212–1221, https://doi.org/10.1007/s11095-007-9499-6.

[34] D.D. Swartz, J.A. Russell, S.T. Andreadis, Engineering of fibrin-based functional and implantable small-diameter blood vessels, Am. J. Physiol. Heart Circ. Physiol. 288 (2005) H1451–H1460, https://doi.org/10.1152/ajpheart.00479.2004.

[35] Z.H. Syedain, L.a. Meier, M.T. Lahti, S.L. Johnson, R.T. Tranquillo, Implantation of completely biological engineered grafts following decellularization into the sheep femoral artery, Tissue Eng. A 20 (2014) 1726–1734, https://doi.org/10.1089/ten.TEA.2013.0550.

[36] Z.H. Syedain, J.S. Weinberg, R.T. Tranquillo, Cyclic distension of fibrin-based tissue constructs: evidence of adaptation during growth of engineered connective tissue, Proc. Natl. Acad. Sci. U.S.A. 105 (2008) 6537–6542, https://doi.org/10.1073/pnas.0711217105.

[37] J.L. Long, R.T. Tranquillo, Elastic fiber production in cardiovascular tissue-equivalents, Matrix Biol. 22 (2003) 339–350, https://doi.org/10.1016/S0945-053X(03)00052-0.

[38] X. Cui, T. Boland, Human microvasculature fabrication using thermal inkjet printing technology, Biomaterials 30 (2009) 6221–6227, https://doi.org/10.1016/j.biomaterials.2009.07.056.

[39] S. Pattanaik, C. Arbra, H. Bainbridge, S.G. Dennis, S.A. Fann, M.J. Yost, Vascular tissue engineering using scaffold-free prevascular endothelial-fibroblast constructs, Biores. Open Access 8 (2019) 1–15, https://doi.org/10.1089/biores.2018.0039.

[40] C.A. Czajka, C.J. Drake, Self-assembly of prevascular tissues from endothelial and fibroblast cells under scaffold-free, nonadherent conditions, Tissue Eng. A 21 (2015) 277–287, https://doi.org/10.1089/ten.TEA.2014.0183.

[41] J.-M. Bourget, R. Gauvin, D. Larouche, A. Lavoie, R. Labbé, F.A. Auger, L. Germain, Human fibroblast-derived ECM as a scaffold for vascular tissue engineering, Biomaterials 33 (2012) 9205–9213, https://doi.org/10.1016/j.biomaterials.2012.09.015.

[42] N. L'Heureux, N. Dusserre, G. Konig, B. Victor, P. Keire, T.N. Wight, N.A.F. Chronos, A.E. Kyles, C.R. Gregory, G. Hoyt, R.C. Robbins, T.N. McAllister, Human tissue-engineered blood vessels for adult arterial revascularization, Nat. Med. 12 (2006) 361–365, https://doi.org/10.1038/nm1364.

[43] J.-Y. Won, M.-H. Lee, M.-J. Kim, K.-H. Min, G. Ahn, J.-S. Han, S. Jin, W.-S. Yun, J.-H. Shim, A potential dermal substitute using decellularized dermis extracellular matrix derived bio-ink, Artif. Cells Nanomed. Biotechnol. 47 (2019) 644–649, https://doi.org/10.1080/21691401.2019.1575842.

[44] V. Lee, G. Singh, J.P. Trasatti, C. Bjornsson, X. Xu, T.N. Tran, S.-S. Yoo, G. Dai, P. Karande, Design and fabrication of human skin by three-dimensional bioprinting, Tissue Eng. C Methods 20 (2014) 473–484, https://doi.org/10.1089/ten.TEC.2013.0335.

[45] W.L. Ng, J.T.Z. Qi, W.Y. Yeong, M.W. Naing, Proof-of-concept: 3D bioprinting of pigmented human skin constructs, Biofabrication 10 (2018) 025005, https://doi.org/10.1088/1758-5090/aa9e1e.

Please cite this article as: S. Freeman, R. Ramos, P. Alexis Chando et al., A bioink blend for rotary 3D bioprinting tissue engineered small-diameter vascular constructs, Acta Biomaterialia, https://doi.org/10.1016/j.actbio.2019.06.052

[46] Y. Shi, T.L. Xing, H.B. Zhang, R.X. Yin, S.M. Yang, J. Wei, W.J. Zhang, Tyrosinase-doped bioink for 3D bioprinting of living skin constructs, Biomed. Mater. 13 (2018) 035008, https://doi.org/10.1088/1748-605X/aaa5b6.

[47] K. Derr, J. Zou, K. Luo, M.J. Song, G.S. Sittampalam, C. Zhou, S. Michael, M. Ferrer, P. Derr, Fully 3D bioprinted skin equivalent constructs with validated morphology and barrier function, Tissue Eng. C Methods (2019), https://doi.org/10.1089/ten.TEC.2018.0318.

[48] T. Hiller, J. Berg, L. Elomaa, V. Röhrs, I. Ullah, K. Schaar, A.-C. Dietrich, M.A. Al-Zeer, A. Kurtz, A.C. Hocke, S. Hippenstiel, H. Fechner, M. Weinhart, J. Kurreck, Generation of a 3D liver model comprising human extracellular matrix in an alginate/gelatin-based bioink by extrusion bioprinting for infection and transduction studies, Int. J. Mol. Sci. 19 (2018) 3129, https://doi.org/10.3390/ijms19103129.

[49] T. Grix, A. Ruppelt, A. Thomas, A.-K. Amler, B.P. Noichl, R. Lauster, L. Kloke, Bioprinting perfusion-enabled liver equivalents for advanced organ-on-a-chip applications, Genes (Basel) 9 (2018) 176, https://doi.org/10.3390/genes9040176.

[50] M. Ali, A.K. Pr, J.J. Yoo, F. Zahran, A. Atala, S.J. Lee, A photo-crosslinkable kidney ECM-derived bioink accelerates renal tissue formation, Adv. Healthc. Mater. 8 (2019) e1800992, https://doi.org/10.1002/adhm.201800992.

[51] K.A. Homan, D.B. Kolesky, M.A. Skylar-Scott, J. Herrmann, H. Obuobi, A. Moisan, J.A. Lewis, Bioprinting of 3D convoluted renal proximal tubules on perfusable Chips, Sci. Rep. 6 (2016) 34845, https://doi.org/10.1038/srep34845.

[52] H.-W. Kang, S.J. Lee, I.K. Ko, C. Kengla, J.J. Yoo, A. Atala, A 3D bioprinting system to produce human-scale tissue constructs with structural integrity, Nat. Biotechnol. 34 (2016) 312–319, https://doi.org/10.1038/nbt.3413.

[53] C. Cvetkovic, R. Raman, V. Chan, B.J. Williams, M. Tolish, P. Bajaj, M.S. Sakar, H. H. Asada, M.T.A. Saif, R. Bashir, Three-dimensionally printed biological machines powered by skeletal muscle, Proc. Natl. Acad. Sci. U.S.A. 111 (2014) 10125–10130, https://doi.org/10.1073/pnas.1401577111.

[54] S. Laternser, H. Keller, O. Leupin, M. Rausch, U. Graf-Hausner, M. Rimann, A novel microplate 3D bioprinting platform for the engineering of muscle and tendon tissues, SLAS Technol. 23 (2018) 599–613, https://doi.org/10.1177/2472630318776594.

[55] Y.-J. Choi, Y.-J. Jun, D.Y. Kim, H.-G. Yi, S.-H. Chae, J. Kang, J. Lee, G. Gao, J.-S. Kong, J. Jang, W.K. Chung, J.-W. Rhie, D.-W. Cho, A 3D cell printed muscle construct with tissue-derived bioink for the treatment of volumetric muscle loss, Biomaterials 206 (2019) 160–169, https://doi.org/10.1016/j.biomaterials.2019.03.036.

[56] N. Diamantides, L. Wang, T. Pruiksma, J. Siemiatkoski, C. Dugopolski, S. Shortkroff, S. Kennedy, L.J. Bonassar, Correlating rheological properties and printability of collagen bioinks: the effects of riboflavin photocrosslinking and pH, Biofabrication 9 (2017) 034102, https://doi.org/10.1088/1758-5090/aa780f.

[57] Q. Gao, Z. Liu, Z. Lin, J. Qiu, Y. Liu, A. Liu, Y. Wang, M. Xiang, B. Chen, J. Fu, Y. He, 3D bioprinting of vessel-like structures with multilevel fluidic channels, ACS Biomater. Sci. Eng. 3 (2017) 399–408, https://doi.org/10.1021/acsbiomaterials.6b00643.

[58] H. Liu, H. Zhou, H. Lan, T. Liu, X. Liu, H. Yu, 3D printing of artificial blood vessel: study on multi-parameter optimization design for vascular molding effect in alginate and gelatin, Micromachines 8 (2017) 237, https://doi.org/10.3390/mi8080237.

[59] H. Liu, H. Zhou, H. Lan, F. Liu, X. Wang, Multinozzle multichannel temperature deposition system for construction of a blood vessel, SLAS Technol. 23 (2018) 64–69, https://doi.org/10.1177/2472630317712221.

[60] J. Sun, H. Tan, Alginate-based biomaterials for regenerative medicine applications, Materials (Basel) 6 (2013) 1285–1309, https://doi.org/10.3390/ma6041285.

[61] E.D. Grassl, T.R. Oegema, R.T. Tranquillo, A fibrin-based arterial media equivalent, J. Biomed. Mater. Res. A 66 (2003) 550–561, https://doi.org/10.1002/jbm.a.10589.

[62] A. Hayashi, S.-C. Oh, Gelation of gelatin solution, Agric. Biol. Chem. 47 (1983) 1711–1716, https://doi.org/10.1080/00021369.1983.10865852.

[63] N. Elharfaoui, M. Djabourov, W. Babel, Molecular weight influence on gelatin gels: structure, enthalpy and rheology, Macromol. Symp. 256 (2007) 149–157, https://doi.org/10.1002/masy.200751017.

[64] Z. Pang, H. Deeth, P. Sopade, R. Sharma, N. Bansal, Rheology, texture and microstructure of gelatin gels with and without milk proteins, Food Hydrocoll. 35 (2014) 484–493, https://doi.org/10.1016/j.foodhyd.2013.07.007.

[65] Z. Pang, H. Deeth, R. Sharma, N. Bansal, Effect of addition of gelatin on the rheological and microstructural properties of acid milk protein gels, Food Hydrocoll. 43 (2015) 340–351, https://doi.org/10.1016/j.foodhyd.2014.06.005.

[66] J. Yin, M. Yan, Y. Wang, J. Fu, H. Suo, 3D bioprinting of low-concentration cell-laden gelatin methacrylate (GelMA) bioinks with a two-step cross-linking strategy, ACS Appl. Mater. Interfaces. (2018), https://doi.org/10.1021/acsami.7b16059.

[67] D.B. Kolesky, K.A. Homan, M.A. Skylar-Scott, J.A. Lewis, Three-dimensional bioprinting of thick vascularized tissues, Proc. Natl. Acad. Sci. U.S.A. 113 (2016) 3179–3184, https://doi.org/10.1073/pnas.1521342113.

[68] S. Wüst, M.E. Godla, R. Müller, S. Hofmann, Tunable hydrogel composite with two-step processing in combination with innovative hardware upgrade for cell-based three-dimensional bioprinting, Acta Biomater. 10 (2014) 630–640, https://doi.org/10.1016/j.actbio.2013.10.016.

[69] A. Tijore, J.-M. Behr, S.A. Irvine, V. Baisane, S. Venkatraman, Bioprinted gelatin hydrogel platform promotes smooth muscle cell contractile phenotype maintenance, Biomed. Microdev. 20 (2018) 32, https://doi.org/10.1007/s10544-018-0274-8.

[70] R. Roeder, J. Wolfe, N. Lianakis, T. Hinson, L.A. Geddes, J. Obermiller, Compliance, elastic modulus, and burst pressure of small-intestine submucosa (SIS), small-diameter vascular grafts, J. Biomed. Mater. Res. 47 (1999) 65–70. http://www.ncbi.nlm.nih.gov/pubmed/10400882.

[71] S. Sinthusamran, S. Benjakul, H. Kishimura, Characteristics and gel properties of gelatin from skin of seabass (Lates calcarifer) as influenced by extraction conditions, Food Chem. 152 (2014) 276–284, https://doi.org/10.1016/j.foodchem.2013.11.109.

[72] T. Huang, Z.-C. Tu, H. Wang, W. Liu, L. Zhang, Y. Zhang, X.-C. ShangGuan, Comparison of rheological behaviors and nanostructure of bighead carp scales gelatin modified by different modification methods, J. Food Sci. Technol. 54 (2017) 1256–1265, https://doi.org/10.1007/s13197-017-2511-1.

[73] E.V.C. da Silva, L.F.H. de Lourenço, R.S. Pena, Optimization and characterization of gelatin from kumakuma (Brachyplatystoma filamentosum) skin, CyTA – J. Food 15 (2017) 361–368, https://doi.org/10.1080/19476337.2016.1266391.

Please cite this article as: S. Freeman, R. Ramos, P. Alexis Chando et al., A bioink blend for rotary 3D bioprinting tissue engineered small-diameter vascular constructs, Acta Biomaterialia, https://doi.org/10.1016/j.actbio.2019.06.052